PARTICLE-LADEN HYPOPYCNAL STRATIFIED SHEAR LAYER: LINEAR STABILITY ANALYSIS

Conference Paper · January 2016

CITATIONS
0

READS
64

2 authors:

Bruno Avila Farenzena
Pontifícia Universidade Católica do Rio Grande do Sul
2 PUBLICATIONS **0** CITATIONS
SEE PROFILE

Jorge Silvestrini
Pontifícia Universidade Católica do Rio Grande do Sul
59 PUBLICATIONS **361** CITATIONS
SEE PROFILE

PARTICLE-LADEN HYPOPYCNAL STRATIFIED SHEAR LAYER: LINEAR STABILITY ANALYSIS

Bruno Avila Farenzena, bruno.farenzena@acad.pucrs.br
Jorge Hugo Silvestrini, jorgehs@pucrs.br
Pontifícia Universidade Católica do Rio Grande do Sul - PUCRS. Av. Ipiranga, 6681 Partenon - Porto Alegre-RS CEP: 90619-900

Abstract. *Gravity-driven riverine outflows are responsible for carrying sediments to the coastal waters, these flows generates some instabilities in the transport of river fresh water into the salty water like the Kelvin-Helmholtz, Holmboe, and settling-driven convection. Results from temporal linear stability analysis of a two layer stratified flow are presented, investigating the behavior of settling particles on the development of streamwise instabilities. The presence of settling particles have basically two effects in the flow: a variation in the Kelvin-Helmholtz mode, and the presence of a settling-driven mode. The settling-driven mode is characterized by a wavelength greater than the Kelvin-Helmholtz mode and can be the most amplified mode for some combination of parameters.*

Keywords: *Linear stability analysis, modal stability, particle-laden flows*

1. INTRODUCTION

Riverine outflows carry more than one-third of land-based precipitation to the oceans. The impact of the terrigenous material transported by these flows into the coastal waters depends on physical processes and transforms the river fresh water as it merges with salty water (Horner-Devine et al., 2015). This transformation process involves stratified-shear mixing caused by instabilities such as Kelvin-Helmholtz ($\mathcal{KH}$), Holmboe ($\mathcal{H}$) and settling-driven convection (Hoyal et al., 1999). These particle-laden flows are usually classified as hypopycnal plumes, resulting in a current along the top of the ocean, or hyperpycnal plumes, generating in a current that follows the bottom of the ocean known also as turbidity currents (Parsons et al., 2001) and are, often, modelled as stratified shear layers (Khavasi et al., 2014).

Most hydrodynamic stability studies in stratified shear layers do not consider the influence of settling particles in suspension. Betchov and Szewczyk (1963) performed a numerical study in the homogeneous shear-layer configuration and found that the Reynolds number, above some critical value, has no influence on the development of the $\mathcal{KH}$ instability allowing the inviscid fluid hypothesis in most of the linear stability works. Hazel (1972) conducted studies in stratified shear flows using the inviscid flow hypothesis and found critical values of Richardson number where the flow is stable and that the $\mathcal{H}$ instability can develop in any shear flow configuration as function of the ratio (R), defined as the relation between the shear layer thickness δ_u and the density layer thickness δ_ρ.

When the settling particles in suspension are considered, Khavasi et al. (2014) investigated the effect of bottom slope, viscosity and particle size in a particle-laden shear layer, where is characterized as a constant value of settling velocity modeled by the Stokes law (Julien, 1998). Among other results, the authors showed that the settling particles does not change the stability characteristics for dimensionless values of particle settling velocity smaller than 10^{-2}. For values greater than 10^{-2}, there is some changes in the instabilities that were not characterized. Based on this, the present study focuses in perform a linear stability analysis in a particle-laden flow where the main objective is the characterization of streamwise instabilities caused by settling particles. The possibility of spanwise instabilities is not considered in present study.

This paper is organized as follows: at section 2 the flow configuration studied is presented; at 3 the governing equations are derived from the continuity, momentum and scalar transport equations; at 4 the numerical methods used to solve the governing equations are described; at 5 the developed computational code is validated; at 6 the results are presented; and lastly, at 7 contains the summary of results and the concluding remarks.

2. FLOW CONFIGURATION

We consider the stability of an unbounded fluid in a vertically stratified velocity and density profiles as sketched in Fig. 1. In this figure, the profile on the left side represents the streamwise velocity with minimum value u^{min}, maximum value u^{max} and shear layer thickness δ_u. The others velocities components are nulls. The profiles on the right side are the total density (solid line), the density added by sediment concentration (dash-dotted line) and the density added by salinity concentration (dashed line) where ρ_0 is the density of clear fluid (this means a fluid without sediment and salinity concentrations) and δ_ℓ (with $\ell = 1$ and 2) are layers thickness associated to the density added by sediment and salinity concentrations respectively.

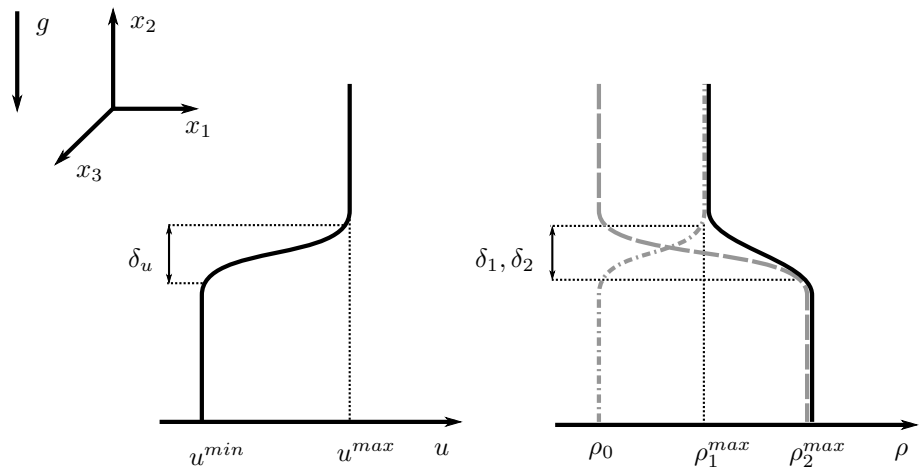

Figure 1. Flow configuration sketch. On the left side, the velocity distribution in the stream-wise direction. On the right side, the density distribution.

The total density is assumed to be a linear function of sediment concentration φ_1 and salinity concentration φ_2:

$$\rho = \rho_0 \left(1 + \sum_{\ell=1}^{2} \gamma_\ell \varphi_\ell \right), \tag{1}$$

where γ_ℓ are the expansion coefficient. In this formulation, it is possible to observe that the values ρ_ℓ^{max} in Fig. 1 are defined by $\rho_0 \gamma_\ell \varphi_\ell^{max}$.

We define a basic state of dimensionless velocity, sediment and salinity concentrations as follows:

$$\bar{u}_1(x_2) = a + \tanh(x_2), \tag{2}$$

$$\bar{\varphi}_1(x_2) = 1 + \tanh(R_1 x_2), \tag{3}$$

and

$$\bar{\varphi}_2(x_2) = 1 - \tanh(R_2 x_2), \tag{4}$$

where a is the a constant mean advection and $R_\ell = \delta_u / \delta_\ell$ is the ratio velocity shear layer thickness δ_u to a concentration thickness δ_ℓ. The profiles are made dimensionless by the use of the scales

$$U = \frac{\Delta u}{2}, \quad L = \frac{\delta_u}{2}, \quad \text{and} \quad \Phi_\ell = \frac{\varphi_\ell^{max}}{2} \tag{5}$$

with $\Delta u = u^{max} - u^{min}$. The choice of hyperbolic tangent for all basic state quantities is justified by a more direct comparison with previous studies results.

3. GOVERNING EQUATIONS

The study of small perturbations growing in the previously described flow configuration, via linear stability theory, requires linearised equations with explicit perturbation fields of flow quantities. These equations are obtained from the continuity, momentum and scalar transport equations by decomposing the flows quantities q_j in a steady part $\bar{q}_j$ (usually called as *basic state* or *base flow*) and in an unsteady part q'_j

$$q_j(x_k, t) = \bar{q}_j(x_k) + \varepsilon q'_j(x_k, t), \tag{6}$$

subtracting the equations for the steady flow and dropping the terms with ε^2 (Juniper et al., 2014). In Eq. (6), ε is a small valued constant. The resulting system of linearised equations from this proceeding, in its dimensionless form, is

$$\frac{\partial u'_j}{\partial x_j} = 0, \tag{7}$$

$$\frac{\partial u'_j}{\partial t} + u'_k \frac{\partial \bar{u}_j}{\partial x_k} + \bar{u}_k \frac{\partial u'_j}{\partial x_k} = \frac{1}{Re} \frac{\partial^2 u'_j}{\partial x_k \partial x_k} - \frac{\partial p'}{\partial x_j} + Ri_2 \left(\frac{1}{R_\rho} \varphi'_1 + \varphi'_2 \right) e_j^g, \tag{8}$$

$$\frac{\partial \varphi_1'}{\partial t} + u_j' \frac{\partial \bar{\varphi}_1}{\partial x_j} + \left(\bar{u}_j + u_s e_j^g\right) \frac{\partial \varphi_1'}{\partial x_j} = \frac{1}{ReSc_1} \frac{\partial^2 \varphi_1'}{\partial x_j \partial x_j} \tag{9}$$

and

$$\frac{\partial \varphi_2'}{\partial t} + u_j' \frac{\partial \bar{\varphi}_2}{\partial x_j} + \bar{u}_j \frac{\partial \varphi_2'}{\partial x_j} = \frac{1}{ReSc_2} \frac{\partial^2 \varphi_2'}{\partial x_j \partial x_j}, \tag{10}$$

where u_j is the fluid velocity, p the pressure, φ_ℓ a scalar concentration, x_k is the space coordinate, t is the time and e_j^g the unity vector in gravity direction, which in this case, is the $-x_2$ direction (Fig. 1). The dimensionless parameters are the Reynolds number (Re), salinity Richardson number (Ri_2), density ratio (R_ρ), Schmidt number (Sc_ℓ) and settling velocity of the particles (u_s). These dimensionless parameters are defined by:

- $$Re = \frac{\Delta u \delta_u}{4\nu}; \tag{11}$$
- $$Ri_2 = \frac{g\gamma_2 \delta_u \varphi_2^{max}}{\Delta u^2}; \tag{12}$$
- $$R_\rho = \frac{\gamma_2 \varphi_2^{max}}{\gamma_1 \varphi_1^{max}}; \tag{13}$$
- $$Sc_\ell = \frac{\nu}{\kappa_\ell}; \tag{14}$$
- $$u_s = \frac{2\tilde{u}_s}{\Delta u}. \tag{15}$$

The base flow is function of coordinate x_2 and, based on this, we may search a solution for the system of equation Eq. (7-10) using a perturbation in form of

$$q_j'(x_k, t) = \hat{q}_j(x_2) e^{i(\alpha x_1 - \sigma t)}, \tag{16}$$

where $\hat{q}_j$ is a amplitude function of a flow variable, α the streamwise wavenumber and σ is a complex number which its real part is the angular frequency and its imaginary part is the growth rate. This formulation of perturbation characterizes a temporal framework because α is a real numbers and σ is a complex number.

Substituting the Eq. (16) in Eqs. (7-10), results in a eigenvalue problem where σ represents eigenvalues and the amplitude function of all flow variables are eigenvectors. With the objective of eliminate the pressure from the system of equations and reduce the size of the eigenvalue problem, one may use a formulation based on the vertical velocity component (u_2) described in the work of Schmid and Brandt (2014). This result in a generalized eigenvalue problem defined by:

$$i(\alpha \bar{u}_1 - \sigma)\mathcal{M}\hat{u}_2 = -i\alpha \frac{d^2 \bar{u}_1}{dx_2^2} \hat{u}_2 + \frac{1}{Re}\mathcal{M}^2 \hat{u}_2 - Ri_2\, \alpha^2 \left(\frac{1}{R_\rho}\hat{\varphi}_1 + \hat{\varphi}_2\right), \tag{17}$$

$$i(\alpha \bar{u}_1 - \sigma)\hat{\varphi}_1 + \frac{d\bar{\varphi}_1}{dx_2}\hat{u}_2 - u_s \frac{d\hat{\varphi}_1}{dx_2} = \frac{1}{ReSc_1}\mathcal{M}\hat{\varphi}_1 \tag{18}$$

and

$$i(\alpha \bar{u}_1 - \sigma)\hat{\varphi}_2 + \frac{d\bar{\varphi}_2}{dx_2}\hat{u}_2 = \frac{1}{ReSc_2}\mathcal{M}\hat{\varphi}_2, \tag{19}$$

where $\mathcal{M}$ is the laplacian operator

$$\mathcal{M} = \frac{d^2}{dx_2^2} - \alpha^2 \tag{20}$$

Considering a sufficiently large domain to avoid boundary perturbations, results in a Dirichlet boundary conditions for all amplitude functions in form of

$$\hat{q}_j(x_2^{min}) = \hat{q}_j(x_2^{max}) = 0. \tag{21}$$

4. NUMERICAL METHODS

To solve the generalized eigenvalue problem described by Eqs. (17-19) is necessary to discretize the spatial derivatives, transform the resulting grid and solve a discrete eigenvalue problem. Is chosen to do the spatial discretization the Chebyshev approximation (Canuto et al., 1988) based in the Chebyshev-Gauss-Lobato (CGL) collocation

$$\hat{y}_j = \cos\left(\frac{\pi j}{N}\right), \quad j = 0, 1, \ldots, N. \tag{22}$$

This differentiation method was implemented in a *Julia* code by adapting a *Differentiation Matrix Suite* routines developed by Weideman and Reddy (2000) in *Matlab* language.

As the CGL collocation corresponds to an orthogonal domain (from -1 to 1), it is necessary to transform the resulting grid into the physical coordinates. This can be done by the mapping function described by Berrut and Mittelmann (2004), it has the form

$$x_2 = \frac{m}{\theta}\tan\left[\text{atan}\left(\theta\right)\hat{y}\right], \tag{23}$$

where x_2 is the coordinate on the real domain, $\hat{y}$ is the CGL points, θ is the point density in a position, which in this case is $y = 0$, and m is the number of characteristics lengths necessary to truncate the domain. The parameter m must be sufficient large to not interfere in the instability development.

The differentiation matrix has also to be transformed to new coordinates by using the chain rule:

$$\mathcal{D} = \hat{\mathcal{D}}\frac{d\hat{y}}{dx_2}, \tag{24}$$

$$\mathcal{D}^2 = \hat{\mathcal{D}}^2\left(\frac{d\hat{y}}{dx_2}\right)^2 + \hat{\mathcal{D}}\frac{d^2\hat{y}}{dx_2^2} \tag{25}$$

and

$$\mathcal{D}^4 = \hat{\mathcal{D}}^4\left(\frac{d\hat{y}}{dx_2}\right)^4 + \hat{\mathcal{D}}^3\left(6\frac{d^2\hat{y}}{dx_2^2}\frac{d\hat{y}}{dx_2}\right) + \hat{\mathcal{D}}^2\left[3\left(\frac{d^2\hat{y}}{dx_2^2}\right)^2 + 4\frac{d^3\hat{y}}{dx_2^3}\frac{d\hat{y}}{dx_2}\right] + \hat{\mathcal{D}}\frac{d^4\hat{y}}{dx_2^4}, \tag{26}$$

where $\hat{\mathcal{D}}^n$ is the differentiation matrix in the orthogonal domain and $\mathcal{D}^n$ is the differentiation matrix in the real domain.

The resulting discrete eigenvalue problem is solved using the `eig` routine from *Julia* based on *Linear Algebra Package* (LAPACK) that applies the *QZ algorithm* (Anderson et al., 1999).

5. VALIDATION CASES

Two cases were chosen to validate the computational code: a homogeneous shear layer and a stratified shear layer. For the first case, the validation is based on the work of Betchov and Szewczyk (1963). The second validation case is based on a comparison with analytical solutions available in Hazel (1972). Both validation cases considers null mean advection ($a = 0$), same layer thickness ratio ($R_\ell = 1$) and do not considers settling of particles ($u_s = 0$).

5.1 Homogeneous shear layer

This configuration is achieved, in the present formulation by setting $Ri_2 = 0$ or $R_\rho = 1$, it means that the total density profile is constant because both $R_\ell = 1$ and consequentially there is no density stratification. This section is organized as follows: a convergence test of growth rate with the mesh parameters N and θ, a verification of Reynolds number dependency and a comparison of maximum growth rate and most amplified wavenumber with results available on the literature.

The Fig. 2a shows the convergence of growth rate increasing the number of rid points. It is observed that the growth rate converges for approximatively 60 grid points. Figure 2b shows the convergence of growth rate increasing the point density parameter and we observe that the growth rate converges at $\theta = 30$. Based on these results, the growth rate is not affected by the mesh parameters N and θ when their values are greater than 60 and 30, respectively.

Figure 3 shows the behaviour of the growth rate and the most amplified wavenumber as a function of Reynolds number. It is observed that for a Reynolds number greater than 10^3, both the growth rate and the most amplified wavenumber are nearly constant reaching 99% of the value for $Re = 10^6$. This means that the viscous effects have no great influence in the development of this instability as it was verified in Betchov and Szewczyk (1963). The growth rate found for $Re = 10^6$ is 0.1897 with corresponding wavenumber of 0.4449. These results present a relative wavenumber error of $-6,74 \times 10^{-4}$ when compared with theory while the growth rate error is null.

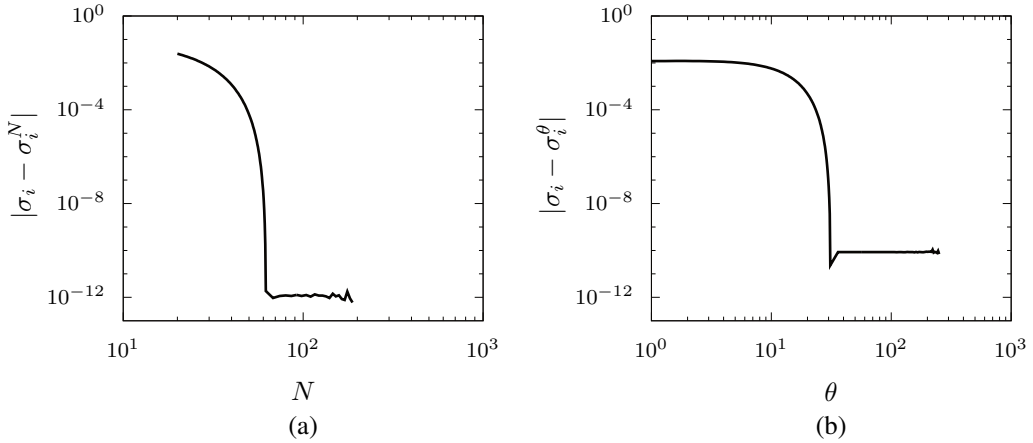

Figure 2. Convergence of σ_i increasing N (a), where σ_i^N is the growth rate for 200 points, and convergence of σ_i increasing θ (b), where σ_i^θ is the growth rate for $\theta = 300$.

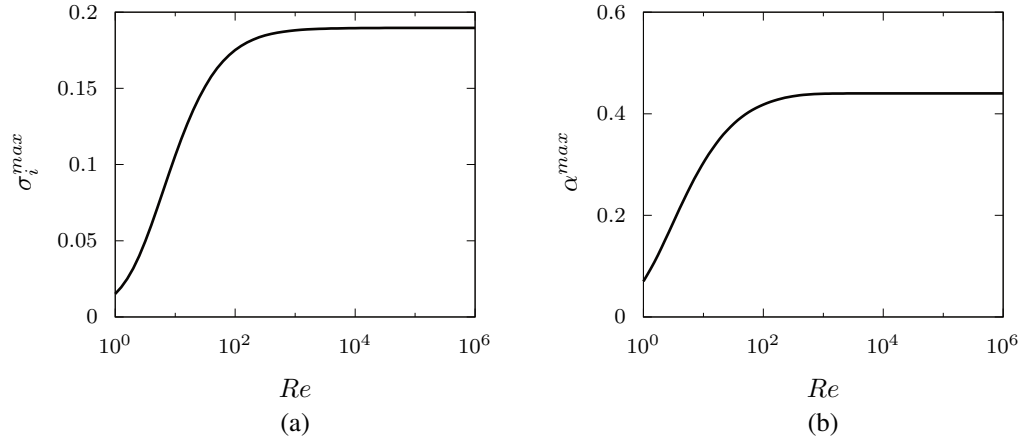

Figure 3. Maximum growth rate (a) and its corresponding wavenumber (b) as function of Reynolds number.

5.2 Stratified shear layer

This configuration have a nonzero salinity Richardson number (Ri_2) and a density ratio (R_ρ) different than one. For hyperpycnal flows this parameter is lower than one and for hypopycnal flows is greater than one. For a better comparison with works available in the literature, R_ρ has to be sufficiently large. This analysis investigates the influence of domain truncation constant m in the stability boundary and results are compared with the analytical solution for inviscid flow ($Re \to \infty$) available in Hazel (1972): $Ri_{SB} = \alpha(1 - \alpha)$.

Figure 4 shows the stability boundary as function of wavenumber, salinity Richardson number and the domain truncation constant m considering a $Re = 10^3$. The stability boundary is deformed by the value of m but the most amplified wavenumber does not change.

In both validation cases, *Kelvin-Helmholtz* is the most amplified growth mode. In present study it will be called $\mathcal{KH}$ mode. $\mathcal{KH}$ mode is more amplified in the streamwise direction and characterized by a wavenumber between 0.4446 and 0.5, depending on the flow stratification, and a angular frequency with valued approximately two times greater than the dimensionless mean advection of the base flow (a). The angular frequency is not showed because the validation cases have a null mean advection.

6. RESULTS

Some problem parameters are fixed in order to reduce the complexity of the analysis, like the base flow parameters (a, R_1 and R_2), the Schmidt numbers of both scalar quantities and the Reynolds number. According Ortiz et al. (2002), the mean advection a in temporal framework acts as a Doppler shift in frequency affecting only the real part of σ, for this reason a is left as zero. The thickness ratio in both concentrations profiles are considered equals to 1 as the *Holmboe* instability is not considered (Hazel, 1972). Both Schmidt numbers are equals to 1 and the Reynolds adopted is 10^3. The

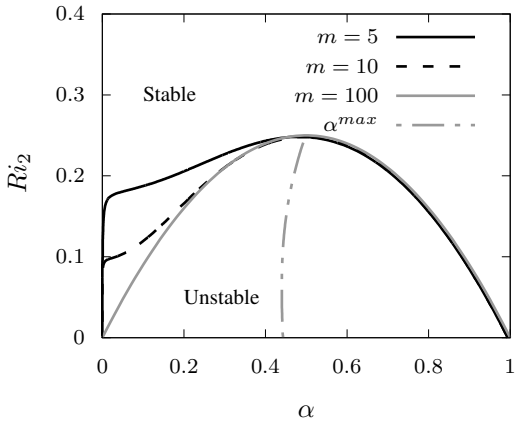

Figure 4. Stability boundaries as a function of streamwise wavenumber and salinity Richardson number for different values of m, where α^{max} is the most amplified wavenumber. Results for $Re = 10^3$.

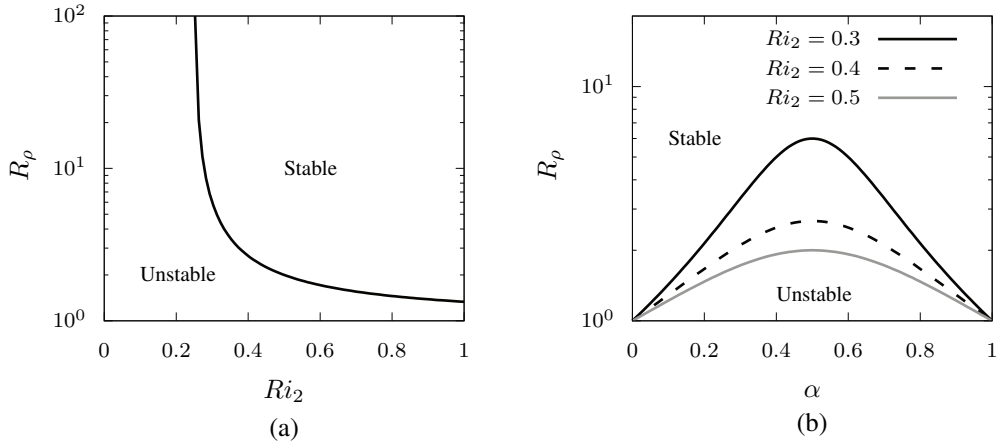

Figure 5. Stability boundary as a function of the salinity Richardson number and density ratio (a) and stability boundary as a function of the streamwise wavenumber and density ratio (b). Results for $Re = 10^3$

parameters investigated are the streamwise wavenumber, the salinity Richardson number, the density ratio and the settling velocity.

6.1 Non-settling configuration ($u_s = 0$)

In a first moment, it is interesting to characterize the instabilities and critical parameters of the base flow for a non-settling configuration ($u_s = 0$). This first analysis has the objective of obtaining base results that will be compared with the results for some settling configurations ($u_s \neq 0$).

Figure 5a presents the stability boundary as a function of salinity Richardson number (Ri_2) and the density ratio (R_ρ). It is observed that when the density ratio is sufficiently large the critical salinity Richardson number is 0.25 (same result as the second validation case). When this parameter has a value equals to or smaller than 0.25 ($Ri_2 \leq 0.25$), the flow is always unstable. On the opposite case ($Ri_2 > 0.25$), the stability of the flow is conditioned by a critical value of density ratio (R_ρ^{crit}). Figure 5b shows the stability boundary as a function of streamwise wavenumber and density ratio for different values of salinity Richardson number. It is observed that these curves are symmetric and centered in $\alpha = 0.5$. The same critical values of density ratio observed in Fig. 5a are verified in Fig. 5b.

The behavior of the maximum growth rate and its corresponding wavenumber as a function density ratio and salinity Richardson number are presented in Fig. 6a and Fig. 6b respectively. The growth rate varies from 0.1893 to zero in the interval of $1 \leq R_\rho \leq R_\rho^{crit}$. The correspondent wavenumber α^{max} for this unstable mode varies from 0.444 to 0.5 in the same interval. The phase velocity, defined as $c_r = \sigma_r/\alpha$, is not presented in Fig. 6 because it is zero for any combination of salinity Richardson number and density ratio. These results characterizes the $\mathcal{KH}$ instability.

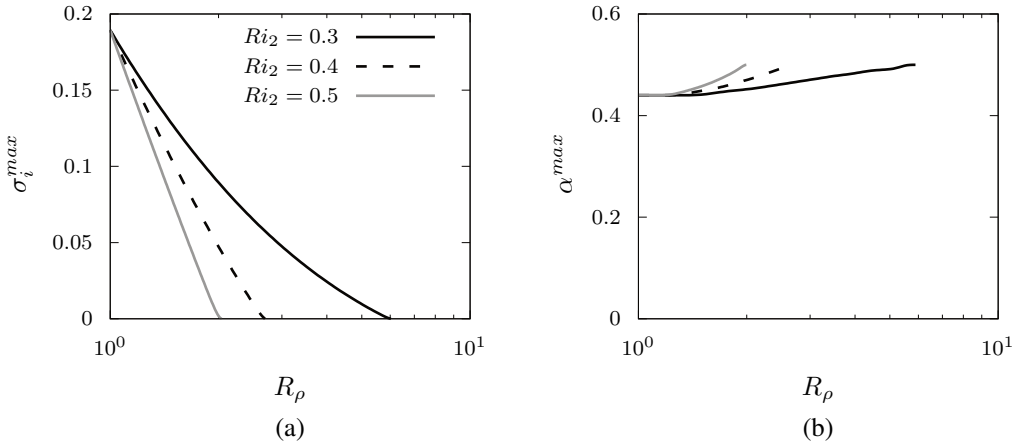

(a) (b)

Figure 6. Maximum growth rate (a) and most amplified wavenumber (b) as a function of density ratio and salinity Richardson number. Results for $Re = 10^3$

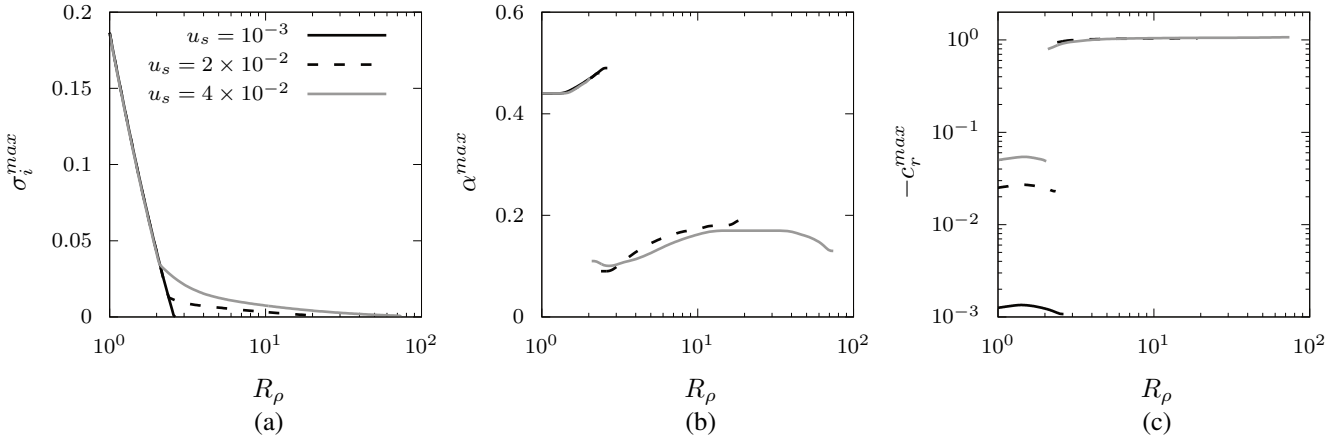

(a) (b) (c)

Figure 7. Maximum growth rate (a), most amplified wavenumber (b) and corresponding phase velocity (c) as a function of the density ratio. Results for $Ri_2 = 0.4$ and $Re = 10^3$.

6.2 Settling configuration ($u_s \neq 0$)

6.2.1 Overview of the instabilities

The presence of settling particles, in this flow configuration, can cause some changes in the $\mathcal{KH}$ mode and amplifies another unstable mode. Figure 7 presents the growth rate (σ_i^{max}), the corresponding wavenumber (α^{max}) and the phase velocity (c_r^{max}) as a function of density ratio for three settling velocities. It is observed that the increment of the settling velocity value dislocates the critical density ratio (Fig. 7a). The discontinuities in Fig. 7b and Fig. 7c are characterized by a competition between two unstable modes (see Fig. 8): the $\mathcal{KH}$ mode ($0.44 < \alpha^{max} < 0.5$) and a settling-driven mode ($0.1 < \alpha^{max} < 0.2$).

The settling-driven mode was not found in the literature and will be denoted in the present study by SD. It is observed that this mode needs a sufficiently large settling velocity value to grow, for example in Fig. 7, the results for $u_s = 10^{-3}$ behaves like non-settling configuration in growth rate and most amplified wavenumber but it has a different phase velocity. A more detailed discussion about the influence of settling particles in the $\mathcal{KH}$ mode and the characteristics of the settling-driven mode are given in the next topics.

6.2.2 How the settling particles affect the Kelvin-Helmholtz instability?

As noted in Fig. 7c, the presence of settling particles (on the $\mathcal{KH}$ mode context) cause some variation in the phase velocity, but, it also cause deformations on the perturbation fields ($\hat{q}_j$). It is important to observe that the maximum growth rate and its correspondent wavenumber does not change.

This variation of the phase velocity is presented in Fig. 9 as a function of the settling velocity. It is observed that this

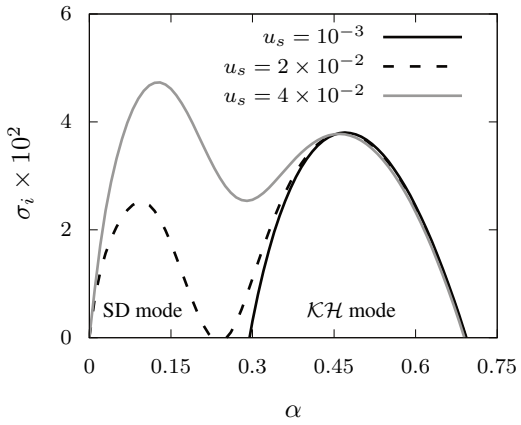

Figure 8. Growth rate as a function of wavenumber for three settling velocities. Results for $Ri_2 = 0.5$, $R_\rho = 1.7$ and $Re = 10^3$.

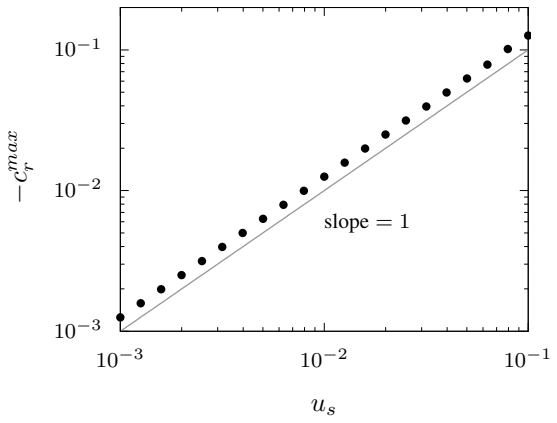

Figure 9. Relation between the phase velocity and the particles settling velocity of the $\mathcal{KH}$ mode. Results for $Ri_2 = 0.4$, $Re = 10^3$ and $R_\rho = 1$.

variation has a linear behavior due to the slope in the graphic, which is equal to -1.

The deformations in the sediment concentration perturbation field are presented in Fig. 10. In this figure, the solid black lines are positive isolines normalized between 0 and 1, the dashed gray lines are negative isolines normalized between -1 and 0, and the x_1 is normalized by it wavelength, defined as $\lambda = 2\pi/\alpha$.

6.2.3 The settling-driven instability

As previously noted, this settling-driven unstable mode needs a sufficiently large settling velocity to grow. This critical value of settling velocity denoted as u_s^{crit}, is a function of the salinity Richardson number. The relation between the critical settling velocity and the salinity Richardson number is presented in Fig. 11, where it is observed, through a fitted function, that these quantities are inversely proportional (slope $= -1.4689$). The correspondent density ratios found for these settling velocity values are the critical density ratio values for a non-settling configuration (see Fig. 5).

Figure 12 shows a comparison of streamwise vorticity (ω_3), defined as

$$\omega_3 = \frac{\partial u_2}{\partial x_1} - \frac{\partial u_1}{\partial x_2}, \tag{27}$$

between the $\mathcal{KH}$ mode (Fig. 12a) and the settling-driven mode (Fig. 12b). Like the previous figures, the solid black lines are positive isolines normalized between 0 and 1, the dashed gray lines are negative isolines normalized between -1 and 0, and the x_1 is normalized by its wavelength.

In the $\mathcal{KH}$ mode, it is observed that the perturbation has the tendency of form vortex in the clockwise sense centered at the point of maximum vorticity ($x_2 = 0$). While in the settling-driven mode, it is observed the tendency of formation of a counter-rotating vortex in approximately $x_2 = -1$.

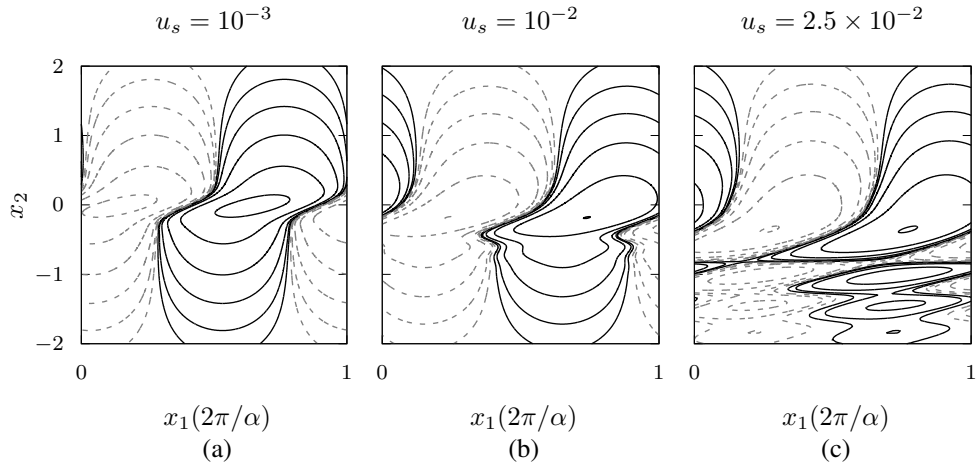

Figure 10. Sediment concentration perturbation field of $\mathcal{KH}$ mode as a function of the particles settling velocity. Results for $Re = 10^3$, $Ri_2 = 0.4$ and $R_\rho = 2$.

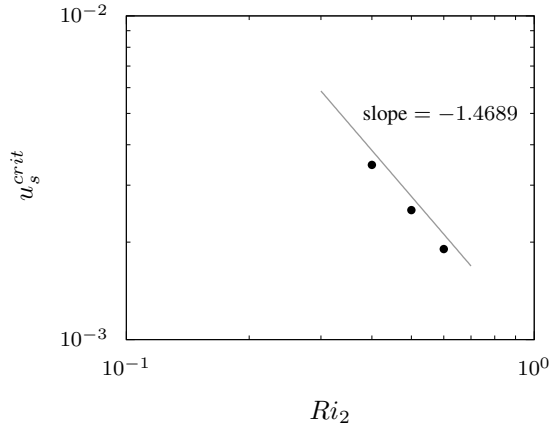

Figure 11. Relation between the salinity Richardson number and the critical settling velocity.

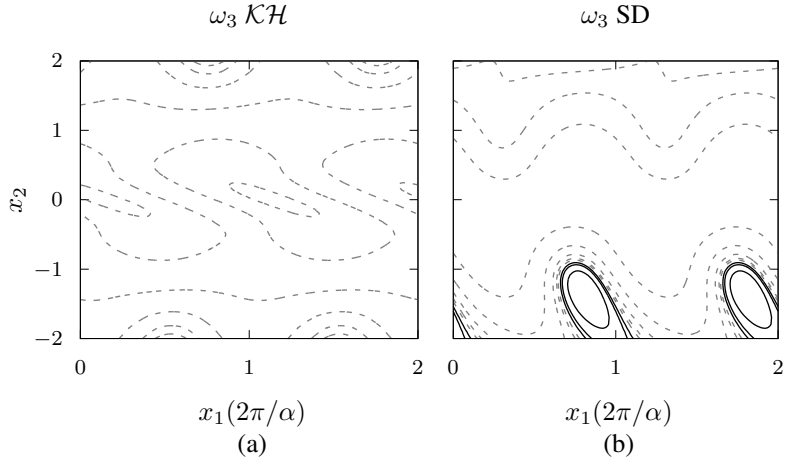

Figure 12. Comparison of perturbation and total fields of streamwise vorticity between the $\mathcal{KH}$ mode and the SD mode. Results for $Re = 10^3$, $Ri_2 = 0.4$, $u_s = 2.5 \times 10^{-2}$ and $\epsilon = 0.5$ (see Eq. 6).

7. SUMMARY AND CONCLUSIONS

A temporal linear stability analysis of a stratified shear flow under action of two scalar volume fractions have been performed in order to investigate the effect of settling particles on the streamwise instabilities developed. This analysis

was based on linearised equations of continuity, Navier-Stokes and scalar transport, Boussinesq approximation and modal perturbation model with invariant basic state over the time. A computational code based on Chebyshev approximation, for the spatial derivatives, and QZ algorithm, to solve the eigenvalue problems, has been developed in *Julia language*. The validation of this code is achieved with results available in the literature.

The settling particles presence have basically two effects on the flow: a variation in the phase velocity and a deformation on the sediment concentration perturbation field of the $\mathcal{KH}$ mode, and amplifying more the new growth mode than the $\mathcal{KH}$ mode for some combinations of parameters (settling velocity, salinity Richardson number and density ratio). These variations in the $\mathcal{KH}$ mode can propitiate the growth of a different mechanism of secondary instabilities. While the settling-driven mode needs a minimal settling velocity to grow and it has a different vortex dynamic.

8. ACKNOWLEDGMENTS

The authors are grateful to Petrobras for supporting this research.

9. REFERENCES

Anderson, E., Bai, Z., Bischof, C., Blackford, L. S., Demmel, J., Dongarra, J. J., Du Croz, J., Hammarling, S., Greenbaum, A., McKenney, A., and Sorensen, D. (1999). *LAPACK Users' Guide (Third Ed.)*. Society for Industrial and Applied Mathematics, Philadelphia, PA, USA.

Berrut, J.-P. and Mittelmann, H. D. (2004). Adaptive point shifts in rational approximation with optimized denominator. *Journal of Computational and Applied Mathematics*, 164165(0):81 – 92.

Betchov, R. and Szewczyk, A. (1963). Stability of a shear layer between parallel streams. *The physics of fluids*, 6(10):1391 – 1396.

Canuto, C., Hussaini, M. Y., Quarteroni, A., and Zang, T. A. (1988). *Spectral methods in fluid dynamics*. Springer series in computational physics. Springer-Verlag.

Hazel, P. (1972). Numerical studies of the stability of inviscid stratified shear flows. *Journal of Fluid Mechanics*, 51:39–61.

Horner-Devine, A. R., Hetland, R. D., and MacDonald, D. G. (2015). Mixing and transport in coastal river plumes. *Annual Review of Fluid Mechanics*, 47(1):569–594.

Hoyal, D. C. J. D., Bursik, M. I., and Atkinson, J. F. (1999). Settling-driven convection: A mechanism of sedimentation from stratified fluids. *Journal of Geophysical Research: Oceans*, 104(C4):7953–7966.

Julien, P. Y. (1998). *Erosion and sedimentation*. Cambridge University Press.

Juniper, M. P., Hanifi, A., and Theofilis, V. (2014). Modal stability theory. *Applied Mechanics Review*, 66(2):024804–.

Khavasi, E., Firoozabadi, B., and Afshin, H. (2014). Linear analysis of the stability of particle-laden stratified shear layers. *Canadian Journal of Physics*, 92(2):103–115.

Ortiz, S., Chomaz, J.-M., and Loiseleux, T. (2002). Spatial holmboe instability. *Phys. Fluids*, 14(8):2585–2597.

Parsons, J. D., Bush, J. W., and Syvitski, J. P. (2001). Hyperpycnal plume formation from riverine outflows with small sediment concentrations. *Sedimentology*, 48(2):465–478.

Schmid, P. J. and Brandt, L. (2014). Analysis of fluid systems: Stability, receptivity, sensitivity. *Applied Mechanics Reviews*, 66.

Weideman, J. A. and Reddy, S. C. (2000). A matlab differentiation matrix suite. *ACM Trans. Math. Softw.*, 26(4):465–519.